SCIENTIFIC REPORTS

OPEN

SUBJECT AREAS:
NANOPARTICLES
METAMATERIALS
ENVIRONMENTAL MONITORING
INFRARED SPECTROSCOPY

Received
2 October 2012

Accepted
4 January 2013

Published
6 February 2013

Correspondence and requests for materials should be addressed to C.V.H. (Hoang.ChungVu@nims.go.jp) or T.N. (Nagao.Tadaaki@nims.go.jp)

Monitoring the Presence of Ionic Mercury in Environmental Water by Plasmon-Enhanced Infrared Spectroscopy

Chung V. Hoang, Makiko Oyama, Osamu Saito, Masakazu Aono & Tadaaki Nagao

WPI Center for Materials NanoArchitectonics (MANA), National Institute for Materials Science, 1-1 Namiki, Tsukuba 305-0044, Japan.

We demonstrate the ppt-level single-step selective monitoring of the presence of mercury ions (Hg^{2+}) dissolved in environmental water by plasmon-enhanced vibrational spectroscopy. We combined a nanogap-optimized mid-infrared plasmonic structure with mercury-binding DNA aptamers to monitor *in-situ* the spectral evolution of the vibrational signal of the DNA induced by the mercury binding. Here, we adopted single-stranded thiolated 15-base DNA oligonucleotides that are immobilized on the Au surface and show strong specificity to Hg^{2+}. The mercury-associated distinct signal is located apart from the biomolecule-associated broad signals and is selectively characterized. For example, with natural water from Lake Kasumigaura (Ibaraki Prefecture, Japan), direct detection of Hg^{2+} with a concentration as low as 37 ppt (37×10^{-10}%) was readily demonstrated, indicating the high potential of this simple method for environmental and chemical sensing of metallic species in aqueous solution.

Mercury emission in the worldwide natural environment has been a pressing problem for many decades. It originates from various sources including the mining industry, burning of fossil fuels and industrial wastes, and volcanic activities[1]. Owing to its volatile nature and long atmospheric residence time, mercury is one of the most serious and ubiquitous hazards in human society. In particular, the Hg^{2+} ion is one of the largest mercuric pollutants in environmental water and should be controlled since it converts into materials that are hazardous to organisms and human health. Since mercury accumulates in the ecosystem during tropospheric cycling, monitoring of very low concentrations of mercury in the early stage of pollution is strongly required for the assessment of hidden risks. Thus far, gas chromatography (GC) and atomic absorption spectroscopy (AAS) are the most sensitive methods for detecting mercury. The detection limit is well below the ppb (10^{-7}% by weight) level but they require dedicated machines for this purpose, and chemical processing for extracting mercury from the as-sampled water is also needed[2]. Various methods have been reported, such as using electrochemical impedance spectroscopy, nuclear magnetic resonance, photoluminescence, and colorimetric sensors, but in most cases, they require several steps for selective detection and the sensitivity is not satisfactory compared with GC and AAS[1,3–6].

Surface plasmon-based optical sensing is one of the most promising techniques since it offers quick, simple, and inexpensive detection with high sensitivity. Among them, surface plasmon resonance (SPR) dielectric sensors enable us simple and quick detection but they do not have a sufficiently high sensitivity in the case of metallic species such as Hg^{2+} [7,8]. On the other hand, plasmon enhanced "vibrational" spectroscopy is an alternative approach that enables us to sensitively detect target species (or guest materials) by monitoring the vibrational state of the linker molecules (or host material)[9,10]. Such sensors, provides us another promising approach with both high selectivity and excellent sensitivity not only for "molecules" but also for "metallic species"[10].

In this report, we present our test-of-concept experiment using of high-efficiency "plasmonic amplifier" to sensitively detect the change in the vibrational state of deoxyribonucleic acid (DNA) aptamer due to Hg-binding.

First, we study the optical property of the gold random nanogap structure. By means of the spectroscopic measurements and numerical simulations, we examine the spectral evolution in the mid-IR of this plasmonic substrate during its morphological development. Secondly, for the application to Hg detection, we use this Au nano-structure as an electromagnetic (EM) amplifier to sense optically the change of the Hg^{2+}-binding DNA aptamers in natural water sampled from Lake Kasumigaura without having any chemical pretreatments. The data taken using a conventional infrared (IR) spectrometer show that the Hg^{2+}-associated sharp IR signal is detected with ppt-level (10^{-10}% by weight) sensitivity separated from the biomolecule-originated signals in the lake water,

thus proving the high potential of this method in chemical and environmental monitoring of metallic species in water.

Results

Role of nanogaps in the molecule-plasmon coupling. In our attenuated total reflection (ATR) setting, the electric field from the free space passes through the silicon crystal and reflects at the water-solid interface, resulting in the so-called evanescent field, with its decay length in the sub-micrometer range. In the presence of the Au nanostructure, this decay length shrinks into the nanometer scale, and the light intensity concentrates on the molecules that cover the Au surface, especially in the nanogaps[11]. Here we utilize this phenomenon to detect trace amounts of target species, by excluding the huge unwanted signal from the bulk water which is the most serious drawbacks in IR spectroscopy.

Figure 1(a) shows a schematic of Hg binding by a DNA aptamer (composed of 15 bases of thymine) immobilized on the Au surface[3,4,8]. First, Hg^{2+} ions are attracted by negatively charged DNA and then go in between two thymine bases by changing the straight single-stranded DNA conformation into hairpin-like (folded)

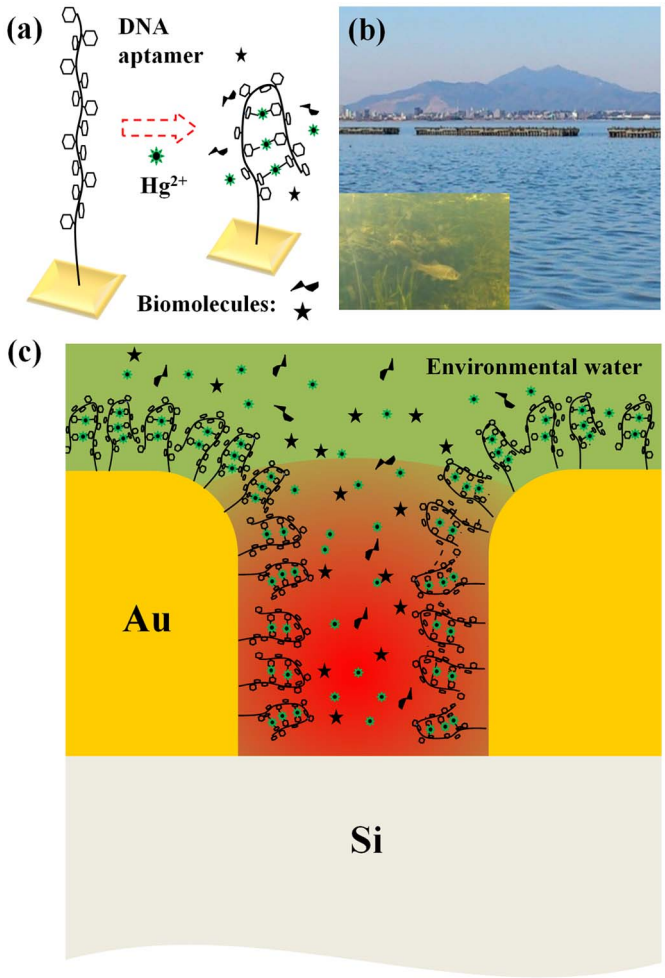

Figure 1 | Mechanism for infrared plasmonic sensing of mercury ions. (a) Schematic of the mercury trapping by a DNA aptamer. A Hg^{2+} ion bridges two thymine bases (small hexagons) and forms N-Hg-N bonds leading to the conformational change of the DNA. (b) A photo of Lake Kasumigaura and subaqueous environment. (c) Schematic of the EM field-enhancement in the Au nanogap (typical gap-size of about 10 nm) with the presence of DNA aptamers on the plasmonic substrate. Structural and chemical changes in these DNA owing to the adsorption of Hg^{2+} ions lead to the modification in the optical spectrum, which later plays as a mechanism for the detection of mercury ions.

structures [Fig. 1(b)]. Also, chemical/electronic status of the local bonds near the trapped Hg between the thymines should undergo substantial change such as change in dipole moment, which manifests itself as a change in vibrational signal intensity[4].

First, to understand the infrared absorption of the plasmonic structure used in this study, we combined the results of *in-situ* IR experiments (see Method) and the numerical electromagnetic (EM) simulations. The rigorous coupled wave analysis method (RCWA method, DiffractMOD, RSoft Design)[12] was used to simulate the influence of the morphological development of nano-particles on their IR response, as well as the spectral coupling of the plasmonic substrate and stretching vibrational signal of water. To precisely simulate the experimental situation, we used typical scanning electron microscopy (SEM) images taken in real experiments in accordance with the growth stages of the plasmonic substrate to simulate the spectra. They are shown in the left of Fig. 2, framed by red, green and blue colors; corresponding height: 15 nm, 25 nm and 40 nm; filling factor: 11%, 52% and 81%, respectively. The dielectric functions in the IR region are taken from the measurements by Johnson and Christy (for Au)[13], and by W. Theiss (for Si and water)[14]. The impinging, polarized (s or p polarization) IR radiation is illuminated from air to the Si substrate, inclined 30° relative to the normal incident of Si. Figure 2a shows the relative reflectance IR spectra of the measured and simulated plasmonic substrates, performed in air. A clear development of the reflectance spectra in the mid-IR is observed as the island's lateral size and the filling factor increase. This evolution shows good accordance with the reports on the lithographic plasmonic objects[15,16]: the red-shift in IR plasmon is induced by the development in the object size and the electromagnetic (EM) coupling between them. In order to verify this simulation result, two typical reflectance spectra are shown. The lower reflectance curve (with circle) corresponds to the film at percolation, showing a good matching with the simulation data. The data at higher reflectance corresponds to the film at the stage slightly before the percolation. It should be noted that the growth conditions between each experiment cannot be exactly the same, a slight variation of the reflectance is often recognized within this range of experiment. A small discrepancy between the simulation and measured data from 3000 cm^{-1} toward higher energy is found which might be either assigned to the surface roughness and roundish corners of real AuNP gap structures, or the much smaller area of the simulated structure than in experiment.

Figure 2b and 2c show the optical property of the Au nano-structures in the presence of water. The *in-situ* IR measurement (Fig. 2b) shows the spectral evolution of the Au nano-structure at different growth stages (three of them are shown by real SEM images on the left). In the very beginning, the relative reflectance spectrum of the initially grown small islands just shows a nearly 100% line, with respect to the initial reference spectrum taken right before the growth of Au nanoparticle (AuNP). This implies that the AuNP resonance does not stay in the IR but in the visible region of the Mie resonance. At further growth stages, the grown AuNPs interconnect and extend laterally, which resemble the situation shown typically in the SEM picture with green frame. Accordingly, as seen in Fig. 2(b), the marked change in the slope of the entire IR spectra coming along with the water (-OH) stretching band (at $\omega_{H_2O} = 3400\ cm^{-1}$) is observed. This evidences the development of laterally grown Au islands and the emergence of the coupled broadband IR plasmon through the physical interconnection and the EM coupling between the islands as discussed above. The enhanced -OH vibrational signal implies that the water vibration starts to hybridize with this broadband IR plasmon. At further growth stages, this -OH stretching vibration evolves into a strongly asymmetric line shape assuming a Fano-type spectral feature. This asymmetric feature is a consequence of the strong hybridization between the broadband plasmonic density of states and the sharp vibrational state of water -OH stretching

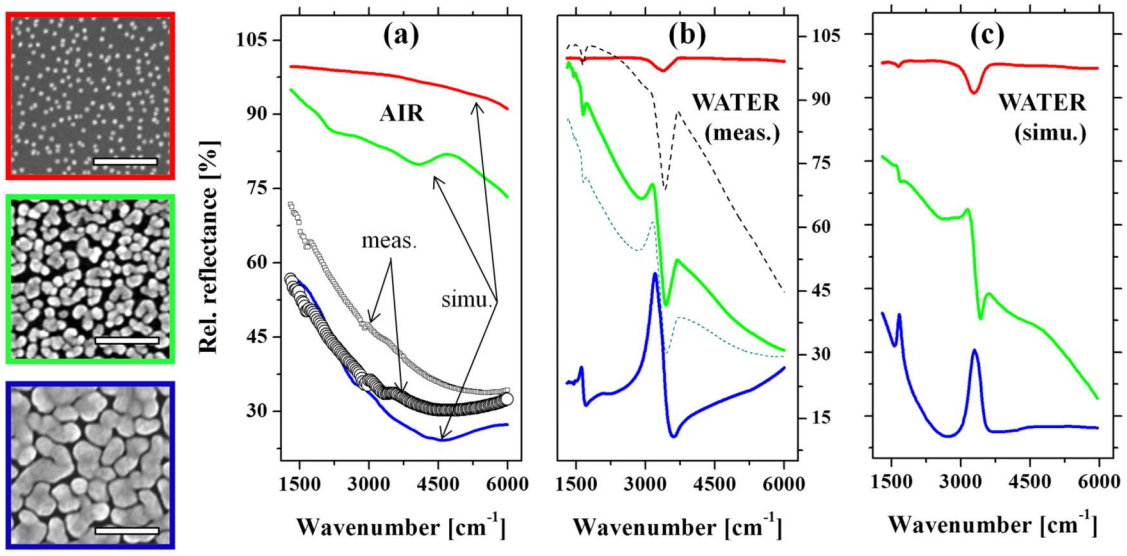

Figure 2 | Experimental and simulated spectra on the optical property of the plasmonic Au nanogap network. On the left: three typical scanning electron microscope (SEM) images of the gold nanostructures, taken at different growth stages, scale bar: 200 nm. Those SEM pictures are used as models for the rigorous coupled wave analysis (RCWA) simulations. (a): A comparison of the simulated spectra (adopting the blue frame SEM) and the measured IR reflectance of the samples whose morphology is similar to that of the SEM pictures in the left. (b): Experimental time evolution of the IR spectra measured *in-situ* during the growth of the AuNP. (c): RCWA simulations of the three growth stages (SEM images in the left) in the presence of water in the nanogaps. The increase of the spectral coupling between the water vibration and the plasmonic excitation of the Au nanostructure could be identified accordingly from the distorted feature of the water bands. The color of each spectrum in (b) and (c) corresponds to each growth stage represented by the SEM images with the same color on the frame.

vibration[17]. The experimental details of the correlation between the spectral feature and the observed surface morphology of the Au nanostructure can be found in a reference[11].

In parallel to the measurement, the RCWA simulations for different growth stages were performed and shown in Fig. 2(c). The presence of water was simulated by incorporating water into the three-dimensional model where the Au nano-islands with various filling factors (see real SEM images on the left) are placed on top of the Si surface and surrounded by water. Good agreements between the experimental data and the simulations are identified accordingly between Fig. 2b and Fig. 2c. Note that the Fano-type spectral shape was reproduced at the stage where the islands nearly touched, but still kept isolated. This confirms that as the gap becomes narrower, the water-plasmon coupling, or hybridization, becomes stronger owing to the interaction through the enhanced EM field at the nanogaps. The ensemble of such a variety of nanoscale planular entities, with a close-packed assembly, exhibits a pronounced broadband resonance extending to the "near- to far-IR" region that overlaps with the entire frequency region of the molecular vibrations.

Optical detection of ionic mercury in natural water. The optical experiments for detecting trace amounts of Hg^{2+} ions were performed by using the following steps. First, after the preparation of the optimized Au nano structure, a 1 μM of thiolated DNA aptamer (in deionized water) solution was introduced into the flow cell for adsorbing the DNA aptamers onto the Au surface. The DNA is composed of 15 bases of thymine and has excellent selectivity for Hg^{2+} against the other ions[3,8]. The strong bonding between the thiol-end group and Au ensures the nearly full coverage of the DNA after the adsorption for 30 min. Subsequently, the natural lake water (sampled from Lake Kasumigaura) was introduced to replace the deionized water. To imitate the lacustrine environment polluted through tropospheric cycling of mercury, the Kasumigaura water was mixed with trace amounts of diluted $HgCl_2$ solutions with different concentrations before introducing into the flow cell.

Figure 3(a) and 3(b) show the relative IR reflectance spectra (in deionized water) after the monolayer adsorption of DNA on the Au

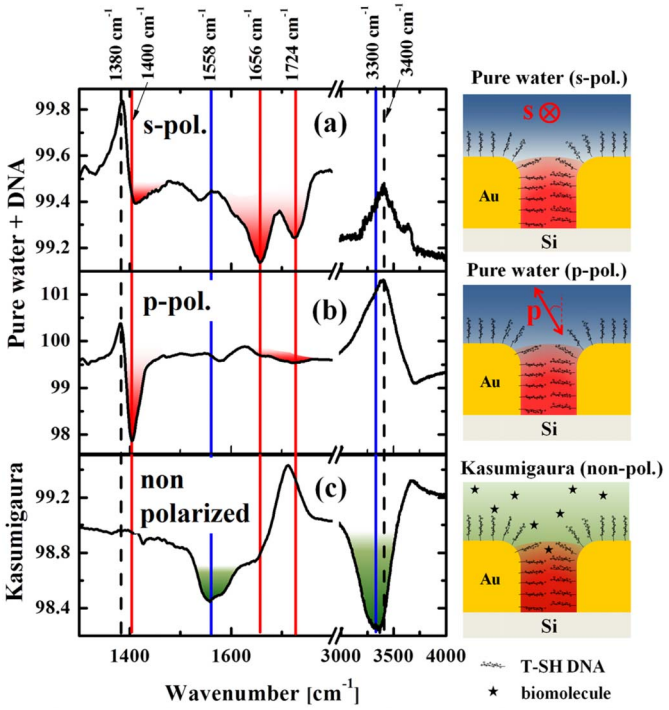

Figure 3 | IR spectra from DNA aptamers. (a) and (b): The relative IR spectra of DNA on AuNP plasmonic structure in pure water under different polarization conditions, s-polarization (a) and p-polarization (b). (c) Measurement performed in sampled water from Lake Kasumigaura. The red and blue features indicate vibrational signals from the DNA and residual biomolecules from Lake Kasumigaura, respectively. Schematic on the right of each graph shows the corresponding depiction of the measurements.

nanostructure recorded with two different polarizations. Two anti-absorption features located at ca. $\omega = 1380$ cm^{-1} and 3400 cm^{-1} are found for both polarizations (as indicated by the two dashed lines in the figures). The former antiabsorption feature corresponds to the desorption of the excess molecules (such as APTES and trisodium citrate) that remained after the fabrication of the Au nanostructure. We often observe this feature during the adsorption of different thiol end-capped molecules, which could be the consequence of the weaker bonding of these residual molecules compared with the strong Au-S bonds. The latter broad feature around $\omega_{H_2O} =$ 3400 cm^{-1} corresponds to the O-H stretching vibration of water, which is gradually replaced by the DNA as they are adsorbed.

Some fingerprint absorption peaks of DNA were clearly observed (indicated by red color), from $\omega = 1400$–1730 cm^{-1}, with strong dependence on the polarization of the incident IR beam. In the case of s-polarization (Fig. 3(a)), C=O and C=C stretching peaks of thymine centered at $\omega = 1656$ cm^{-1} and 1724 cm^{-1} (signal intensity of 0.2%) were observed[18–21]. In the case of p-polarization (Fig. 3(b)), absorption line at $\omega_T = 1400$ cm^{-1} was clearly observed with higher intensity (1.8%). In contrast to the weaker signal reported for the case of free-standing thymine DNA in water[21], the absolute dominance of this peak with strong anisotropy may be an indication of the good alignment of the DNA with respect to the Au surface. If this is the case, this can be partly due to its unique base sequence solely composed of thymine, where the straight anisotropic conformation of the DNA readily takes place. Near the saturation coverage, the self-assembly of the DNA will take place owing to their high packing density as well as to the Coulombic repulsion between the negatively charged DNA molecules.

Since the EM field from the incident IR light is strongly concentrated inside the Au nanogaps[22], the observed vibrational features mostly originate from the DNA aptamers assembled therein, aligned perpendicular to the side walls of nanogaps (as a simple assumption). If this is the case, the difference of the IR signals found for the polarization dependent measurements may be an indication of a polarization dependence of this vertically aligned DNA molecules. A similar investigation for the alignment of water molecules at the water-metal interface had also been reported in literature[23] providing the difference of IR signals between interfacial water and bulk water. For the roundish-like DNA structures whose configuration is more isotropic, such polarization dependence was not found[24].

It should be noted that the antenna resonance of the plasmonic substrate gives strong near-field EM field confinement in the nanogaps mostly with the surface-parallel direction for both polarizations. In the case of s-polarization, the electric field of the incident light is aligned perpendicular to the surface of the nanogaps and the DNAs in the gaps are excited along their long axes. In contrast, the electric field of the p-polarized light is inclined 30° from the normal direction of the Si surface and can result in slightly different (weaker) electric field intensity in the gap as well as on top of the Au island surfaces. Such difference might result in a different spectral feature as can be contrasted in Figs. 3(a) and (b).

Figure 3(c) shows the relative IR spectrum of the Kasumigaura water normalized to the initial spectrum of DNAs in pure deionized water (no polarizer used). After 16 h, we did not observe any noticeable change in the thymine-related peak at $\omega_T = 1400$ cm^{-1}, revealing that the structural component related to this vibration is very stable and remains unchanged even after the exposure to the as-sampled natural lake water.

In contrast to the invariance of this DNA-associated feature, biomolecule-related vibrational bands emerge, indicating their abundance in the lacustrine environment: two broad peaks located at ~1558 cm^{-1} (α: C-N stretching and N-H bending modes, Amide II), a shoulder at ~1656 cm^{-1} (β: C=O Amide I) and ~3300 cm^{-1} (γ: N-H stretching mode). These spectral features are in accordance with the positions expected from amino acids (also fatty acids and aldoses), which exist as major components produced through microbial decomposition in Lake Kasumigaura[25].

Figure 4 shows the evolution of relative IR spectra taken from the natural lake water mixed with different Hg^{2+} concentrations. The reference spectrum was taken from the original lake water before mixing with a trace amount of Hg^{2+}. Each spectrum was accumulated for 30 min to ensure the near saturation of the mercury adsorption. In contrast to the spectrum of the original natural lake water without Hg^{2+} (Fig. 3(c)), we clearly observed the evolution of the peak at $\omega_T = 1400$ cm^{-1} (marked as red, solid line), which systematically changed its intensity depending on the Hg^{2+} concentration. The peak shape remains unchanged with different concentrations. Also no shift in the peak position was observed. This intensity change was not observable from the water without Hg^{2+} and only observed from the Hg containing solutions. Also we did not observe the changes in C=O and C=C bands at $\omega = 1656$ cm^{-1} and 1724 cm^{-1} indicating that the DNA itself did not desorb from the surface.

Figure 5(a) shows a schematic of the DNA aptamers after the absorption of Hg^{2+}, according to the model reported in the literature[3,4,8]. Owing to the absorption of Hg^{2+}, the DNA aptamers can fold their shape from straight to hairpin-like geometry, giving rise to the distortion of their straight and highly anisotropic feature. The microscopic driving force of this change is the connection of two thymine

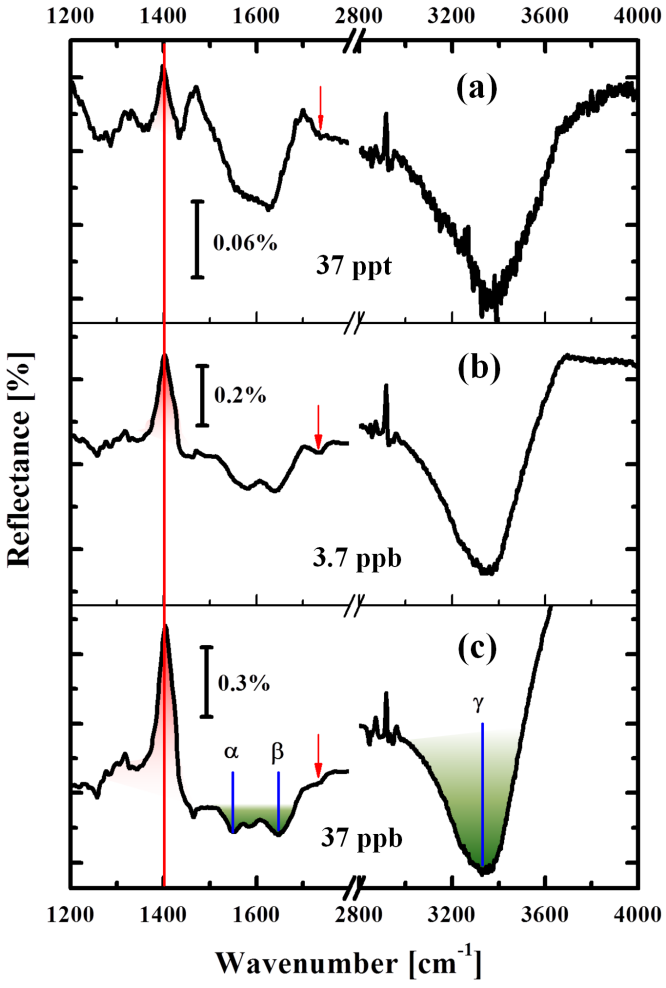

Figure 4 | Detection of the presence of ionic mercury in environmental water. Spectral evolution shown as a function of Hg^{2+} concentration (added into water of Lake Kasumigaura). DNA-related signal is indicated by red peak and small red arrows. Green absorption feature shows the residual biomolecules in the lake water. Note that the scale of reflectance is different for each sub-graph.

bases bridged by a Hg^{2+} ion. As shown in Fig. 5(a) (right) the new N-Hg^{II}-N bond is formed by releasing two imino protons into the solution[4]. This process accompanies with the substantial charge re-distribution near the two N atoms in the imide structures (surrounded by red dotted square), and subsequently leads to the intensity change of the vibrational peak at ω_T = 1400 cm^{-1}. Since this mode involves large displacement of the N atom in the imide structure[18–20], the observed antiabsorption peak at ω_T = 1400 cm^{-1} is most possibly associated with the vibrational mode involving this N atom which sensitively reflects the dipole moment change owing to the formation of N-Hg^{II}-N bonds. On the other hand, C=O related band at ω = 1724 cm^{-1} in the same imide structure shows only slight increase in the absorption intensity (indicated by small red arrows in Fig. 4) suggesting that very small charge re-distribution occurs for the atoms further than the second nearest-neighbor from the Hg^{II} atom.

In the meantime, simultaneous increases in the biomolecule-related IR absorption lines at: α: 1558 cm^{-1}, β: 1656 cm^{-1} and γ: 3300 cm^{-1} are observed. The normalized signal intensity for these vibrational features plotted as a function of Hg^{2+} concentration is shown in Fig. 5(b). The signal intensities for all these four vibrational modes show the same behavior, indicating that the adsorption kinetics of all these components are the same. This means that the biomolecules enter the Au nanogaps simultaneously as the Hg^{2+} adsorption proceeds: the structural folding of DNA aptamers will provide a space for the biomolecules to enter more into the Au gaps, which enhances their absorption signals substantially. It should be noted that the thymine-Hg^{II}-related signal at ω_T = 1400 cm^{-1} is energetically well separated from these biomolecule signals, and we readily obtained the ppt-level spectral-response by directly measuring the lake water without any chemical pretreatment. This is a clear advantage over many other techniques, where some chemical processing steps are normally required before measurements[2].

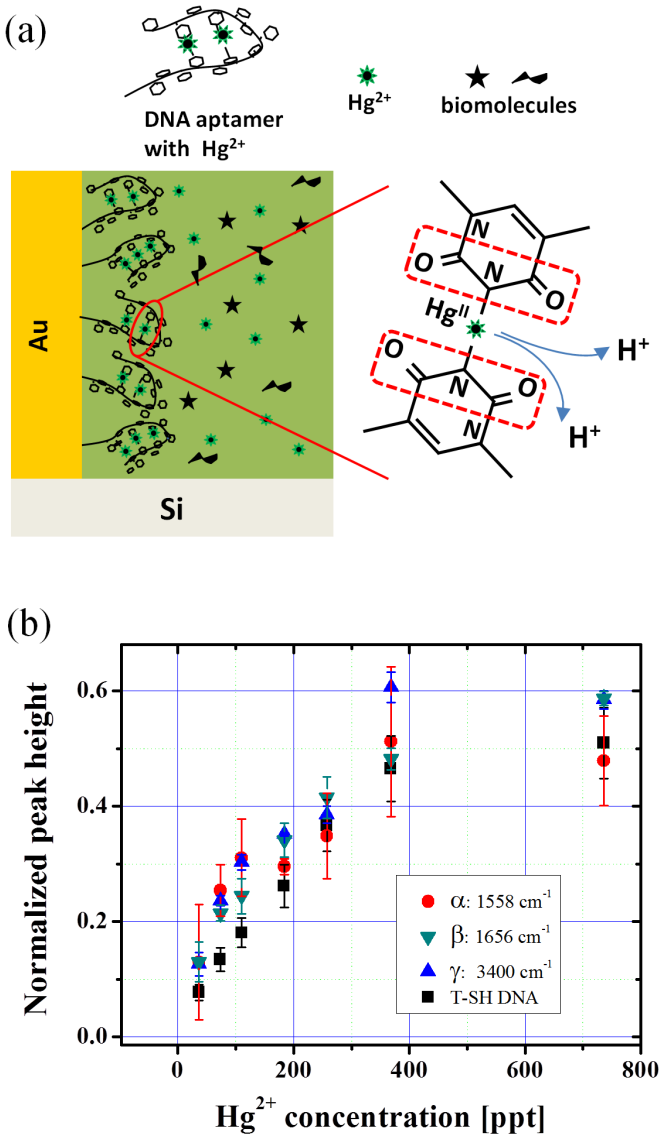

Figure 5 | (a) Schematic of the structural deformation of DNA owing to the bridge-site adsorption of Hg^{2+} in the presence of different biomolecules occupying the in-gap space near the folded DNA. Two thymine bases are bridged by an Hg^{2+} ion after releasing two imino protons. Subsequently the neighboring bonds around the N atoms in the imide structures (marked by red dotted frame) will modify its dipole moment and gives rise to the IR signal change. (b) Evolution of the intensity of the DNA peak (related to the imide bond in thymine) at ω = 1400 cm^{-1} and biomolecule-related ones at α: 1558 cm^{-1}, β: 1650 cm^{-1} and γ: 3300 cm^{-1}, by varying the Hg^{2+} concentration.

Discussion

Compared with previous works on mercury detection using optical sensors, this random nanogap structure realizes an improved sensitivity and quick detection. It is surprising that a very low concentration of Hg^{2+} (as low as 37 ppt) was optically detected in the as-sampled lake water using a standard FT-IR spectrometer. The greatest advantage here is that there is neither need for a dedicated machine nor chemical pretreatment to extract the mercury from other background components. By taking advantage of the inherent spectral separation between the mercury-sensitive signal and the biomolecule-originated signal in vibrational spectroscopy, selective detection of ionic mercury from environmental water is possible, which also indicates the high potential of this simple methodology in environmental monitoring and various chemical sensing.

In conclusion, we have proposed an *in-situ* plasmonic sensing that is cost-effective, simple, and potentially applicable onsite for environmental monitoring of ionic mercury. The key features of the sensor material are the high density of nanogaps and their randomness, which make the Au nanostructures act as a mid-infrared EM amplifier and enhance the vibrational signal of the mercury-binding DNA aptamer. The Hg^{2+}-associated signal was extracted selectively from the signals of residual biomolecules that exist as major components in the lacustrine water. Our first attempt using a conventional FT-IR spectrometer already exhibited very high sensitivity down to the ppt level (10^{-10}% level). Further improvements such as combining with aptamers for different metallic species and adopting portable IR spectrometers will make this method more ubiquitous and suitable for the onsite applications in environmental monitoring, laboratory chemical research, and quality management in industry.

Methods

Optical set-up. The experiments were performed with a standard Fourier transform infrared (FT-IR) spectrometer (Nicolet-Japan NEXUS-670) equipped with a mercury cadmium telluride (MCT) detector, a KBr beam splitter, and a custom-made liquid flow cell[11]. The IR measurements were carried out in the attenuated total reflectance (ATR) geometry, with a resolution of 4 cm^{-1}, under an appropriate (s- or p-) polarization condition. The incident angle of the IR beam was 30°, inclined relative to the normal direction of the silicon sample.

Preparation of infrared Au nanostructures coated with DNA aptamers. The Si ATR crystal with a natural SiO_2 layer was exposed to 10% [aminopropyltriethoxysilane (APTES) - methanol] solution for 30 min. Subsequently, a droplet of 11-nm-diameter Au nanoparticle (AuNP) suspension was deposited onto the APTES surface to form a sub-monolayer Au nucleus. Subsequently the AuNP sub-monolayer was grown by exposing to a Au^{3+}/NH_2OH solution [0.3 mM $HAuCL_4$ (Aldrich) and 0.4 mM NH_2OH (Acros Organics)] in water at a constant flow rate of 3 $ml.min^{-1}$. The IR spectra were recorded during the growth of the AuNP film to investigate and control *in-situ* the optical development of

the film. We controlled the final stage of the film by looking at the coupling strength of the water vibration ($\omega_{H_2O} = 3400 cm^{-1}$) and the broadband plasmonic excitation in the nanostructured gold substrate (see Fig. 4(a)).

The 1 μM solution (10 ml in volume) of thiol-functionalized single-stranded DNA oligonucleotide with 15 bases of thymine [5′-SH-(CH_2)6-TTT TTT TTT TTT TTT-3′] (Life Technology Japan Ltd.) was prepared by solving DNA in de-ionized water (resistivity $\rho > 18.4$ MΩ·cm). This solution was subsequently treated in an oil bath at 95°C for 10 min, followed by a slow temperature decrease to 65°C and naturally cooled to room temperature. The DNA solution was then introduced into the ATR flow cell with Au nano-structure and the DNA monolayer is immobilized on the Au surface.

Preparation of environmental water with controlled Hg^{2+} concentration. The environmental water was sampled from Lake Kasumigaura (Ibaraki Prefecture, Japan) and used as solvent for the experiments after being filtered with filter paper (5 μm pore size) to remove particulates. The mercury detection experiment was performed by diluting Hg^{2+} ($HgCl_2$ Sigma Aldrich) in the environmental water and introducing into the ATR flow cell with DNA/Au nanostructures. Fraction of the Hg^{2+} ions with respect to the other components ($HgCl_2$ and $HgCl^+$) in aqueous solution varies depending on the ionization equilibrium. In the concentration region used in our work (ppt region), the Hg^{2+} ion is the largest mercuric component.

1. Nolan, E. M. & Lippard, S. J. Tools and tactics for the optical detection of mercuric ion. *Chem. Rev.* **108**, 3443–3480 (2008).
2. Ministry of the environment, Japan. "Mercury analysis manual". *National Institute for Minamata Disease* website; http://www.nimd.go.jp/english/kenkyu/docs/2004_march_mercury_analysis_manual(e).pdf Date of access: October 3, 2012.
3. Cao, R. G., Zhu, B., Li, J. & Xu, D. Oligonucleotides-based biosensors with high sensitivity and selectivity for mercury using electrochemical impedance spectroscopy. *Electrochem. Commun.* **11**, 1815–1818 (2009).
4. Miyake, Y., Togashi, H., Tashiro, M., Yamaguchi, H., Oda, S., Kudo, M., Tanaka, Y., Kondo, Y., Sawa, Y., Fujimoto, T., Machinami, T. & Ono, A. $Mercury^{II}$-mediated formation of thymine−Hg^{II}−thymine base pairs in DNA duplexes. *J. Am. Chem. Soc.* **128**, 2172–2173 (2006).
5. Yang, Y.-K., Yook, K.-J. & Tae, J. A rhodamine-based fluorescent and colorimetric chemodosimeter for the rapid detection of Hg^{2+} ions in aqueous media. *J. Am. Chem. Soc.* **127**, 16760–16761 (2005).
6. Lee, J. S., Han, M. S. & Mirkin, C. A. Colorimetric detection of mercuric ion (Hg^{2+}) in aqueous media using DNA-functionalized gold nanoparticles. *Angew. Chem. Int. Ed.* **46**, 4093–4096 (2007).
7. Liu, C. W., Huang, C. C. & Chang, H. T. Control over surface DNA density on gold nanoparticles allows selective and sensitive detection of mercury(II). *Langmuir* **24**, 8346–8350 (2008).
8. Wang, L., Li, T., Du, Y., Chen, C., Li, B., Zhou, M. & Dong, S. L. Au NPs-enhanced surface plasmon resonance for sensitive detection of mercury(II) ions. *Biosens. Bioelectron.* **25**, 2622–2626 (2010).
9. Liu, N., Tang, M. L., Hentschel, M., Giessen, H. & Alivisatos, A. P. Nanoantenna-enhanced gas sensing in a single tailored nanofocus. *Nat. Mater.* **10**, 631–636 (2011).
10. Neubrech, F., Pucci, A., Cornelius, T. W., Karim, S., García-Etxarri, A. & Aizpurua, J. Resonant plasmonic and vibrational coupling in a tailored nanoantenna for infrared detection. *Phys. Rev. Lett.* **101**, 157403–157407 (2008).
11. Enders, D., Nagao, T., Pucci, A., Nakayama, T. & Aono, M. Surface-enhanced ATR-IR spectroscopy with interface-grown plasmonic gold-island films near the percolation threshold. *Phys. Chem. Chem. Phys.*, **13**, 4935–4941 (2011).
12. *RSOFT Design Group* website; http://www.rsoftdesign.com/products.php?sub=Component+Design&itm=DiffractMOD. Date of access: October 3, 2012.
13. Johnson, P. B. & Christy, R. W. Optical constants of the noble metals. *Phys. Rev. B* **6**, 4370–4379 (1972).
14. *W. Theiss Hard and Software* website; http://www.wtheiss.com/?c=1&content=scout, or http://www.techno-synergy.co.jp/. Date of access: October 3, (2012).
15. Weber, D., Albella, P., Alonso-González, P., Neubrech, F., Gui, H., Nagao, T., Hillenbrand, R., Aizpurua, J. & Pucci, A. Longitudinal and transverse coupling in infrared gold nanoantenna arrays: long range versus short range interaction regimes. *Opt. Express* **19**, 15047–15061 (2011).
16. Chu, Y., Schonbrun, E., Yang, T. & Crozier, K. B. Experimental observation of narrow surface plasmon resonances in gold nanoparticle arrays. *Appl. Phys. Lett.* **93**, 181108 (2008).
17. Nagao, T., Han, G., Hoang, C. V., Wi, J. S., Pucci, A., Weber, D., Neubrech, F., Silkin, V. M., Enders, D., Saito, O. & Rana, M. Plasmons in nanoscale and atomic-scale systems. *Sci. Technol. of Adv. Mater.* **11**, 054506 (2010).
18. Tsuboi, M., Takeuchi, Y., Kawashima, E., Ishido, Y. & Aida, M. Raman and infrared spectra of (2′S)-[2′-H-2. thymidine-vibrational coupling between deoxyribosyl and thymine moieties and structural implications. *J. Am. Chem. Soc.*, **119**, 2025–2032 (1997).
19. Rush, T. III. & Peticolas, W. L. Ab initio transform calculation of resonance raman spectra of uracil, 1-methyluracil, and 5-methyluracil. *J. Phys. Chem.* **99**, 14647–14658 (1995).
20. Rastogi, V. K., Singh, C., Jain, V. & Palafox, M. A. FTIR and FT-Raman spectra of 5-methyluracil (thymine). *J. Raman Spectrosc.* **31**, 1005–1012 (2000).
21. Schreier, W. J., Schrader, T. E., Koller, F. O., Gilch, P., Crespo-Hernández, C. E., Swaminathan, V. N., Carell, T., Zinth, W. & Kohler, B. Thymine dimerization in DNA is an ultrafast photoreaction. *Science* **315**, 625–629 (2007).
22. Schnell, M., García-Etxarri, A., Huber, A. J., Crozier, K., Aizpurua, J. & Hillenbrand, R. Controlling the near-field oscillations of loaded plasmonic nanoantennas. *Nat. Photonics* **3**, 287–291 (2009).
23. Hasegawa, T., Nishijo, J., Imae, T., Huo, Q. & Leblanc, R. M. *J. Phys. Chem. B* **105**, 12056–12060 (2001).
24. Hoang, C. V., Oyama, M., Saito, M., Enders, D., Aono, M. & Nagao, T. paper in preparation.
25. Hanamachi, Y., Hama, T. & Yanai, T. Decomposition process of organic matter derived from freshwater phytoplankton. *Limnology* **9**, 57–69 (2008).

Acknowledgements

This work was supported by a Grant-in-Aid for Scientific Research (KAKENHI) from the Japan Society for the Promotion of Science (JSPS) and World Premier International Research Center Initiative on "Materials Nanoarchitectonics" from MEXT (Japan). C.V.H acknowledges the fellowship program of JSPS.

Author contributions

T.N. supervised the project. C.V.H. and M.O. conducted the experiment. O.S., T.N. and C.V.H. performed the EM simulations. C.V.H. analyzed the data and co-wrote the manuscript with T.N. All the authors discussed and commented on the manuscript.

Additional information

Competing financial interests: The authors declare no competing financial interests.

How to cite this article: Hoang, C.V., Oyama, M., Saito, O., Aono, M. & Nagao, T. Monitoring the Presence of Ionic Mercury in Environmental Water by Plasmon-Enhanced Infrared Spectroscopy. *Sci. Rep.* **3**, 1175; DOI:10.1038/srep01175 (2013).